Chapter 12

On yielding, failure, and softening response of rock

J.F. Labuz[1], R. Makhnenko[2], S-T. Dai[3] & L. Biolzi[4]
[1]*University of Minnesota, Minneapolis, USA*
[2]*University of Illinois at Urbana-Champaign, USA*
[3]*Minnesota Department of Transportation, USA*
[4]*Politecnico di Milano, Italy*

Abstract: Mechanical descriptors of inelastic behavior of rock are reviewed and approaches to measure material and system response are highlighted. A non-traditional testing method that involves biaxial deformation developed through a Vardoulakis-Goldscheider plane strain apparatus is used to assess dilatancy and friction, as well as dilatancy of the shear band after localization. The Paul-Mohr-Coulomb failure criterion, which includes the intermediate stress, is applied to interpret the experiments at peak stress. Post-peak response, often referred to as softening, is explained as a size effect within the context of class I-class II stability.

This chapter is dedicated to I. Vardoulakis (1949–2009), a giant of modern geomechanics

1 INTRODUCTION

"In discussions with sensible professional men, I have not infrequently encountered the opinion expressed that it would be wasting vain efforts to develop a theory on which the strength of materials could be based scientifically. Homogeneous bodies of materials – I was told – do not exist, homogeneous states of stress are not encountered. It seems, therefore, utterly impossible to deduce a law of nature from experience. Since the existing irregularities furthermore are of such a nature that they nearly completely obscure any orderly behavior, it has little interest to track down the half-blurred traces of such laws. Under these circumstances nothing else remains than to make special tests in every case and to pay no heed to a physical interpretation of the results. I had to admit in each case that nothing could be said against this reasoning; and yet for more than one hundred years, there have been attempts again and again to establish order within the confusing abundance of the experiences. If one should succeed in finding a few rules under which many experiences could be subordinated – of course rules in which some confidence can be placed – no law of nature would have been derived, but some means found for judging the probability of new results of experience" (Mohr, 1901; from Nadai, 1950).

Rock is a complex material exhibiting, to various degrees, heterogeneity, anisotropy, pressure dependence, and irreversible damage. Nevertheless, extraordinary structures in (or of) rock have been designed and built, and general rules regarding their mechanical response have been identified (Vardoulakis & Sulem, 1995). In fact, when numerous observations from experiments on different rock types are compared, it is soon discovered that rock behaves in a similar manner from certain points of view. If the

correct variables are used to measure material properties, then many phenomena can be explained by identical relations, *e.g.* Mohr-Coulomb failure criterion.

Concepts associated with the measurement of mechanical properties of rock are reviewed. As in many branches of engineering, specific tests have evolved for evaluation of response under conditions of interest; examples of tests in geomechanics are conventional triaxial compression or extension and plane strain compression. Furthermore, general behavior of a dilatant, frictional rock is highlighted and experimental results of interest are discussed.

2 PLANE STRAIN APPARATUS

An apparatus for determining the constitutive and failure response of rock, named the University of Minnesota Plane Strain Apparatus (Labuz *et al.*, 1996), was designed and built based on a passive stiff-frame concept of Vardoulakis & Goldscheider (1981). The biaxial device, in the sense of plane strain deformation, is unique because it allows the failure plane to develop and propagate in an unrestricted manner (Drescher *et al.*, 1990). By placing the upper platen on a low friction linear bearing, the prismatic specimen has the freedom to translate in the lateral direction if the deformation has localized. A schematic of the Apparatus is shown in Figure 1. A prismatic specimen 75–100 mm in height h, 27–40 mm in width w, 100 mm in length b, is placed within a stiff biaxial frame; the thick-walled cylinder limits the deformation of the specimen to very small values, approximating the plane strain condition (Makhnenko & Labuz, 2014). The specimen is subjected to lateral (confining) pressure by placing the entire assembly within a pressure vessel, and to axial load applied through displacing rigid platens by a servo-hydraulic actuator. In contrast to other plane strain devices with similar loading conditions, the upper loading platen is attached to a linear bearing. The low friction bearing allows free displacement of the upper part of the specimen upon formation of a failure mechanism

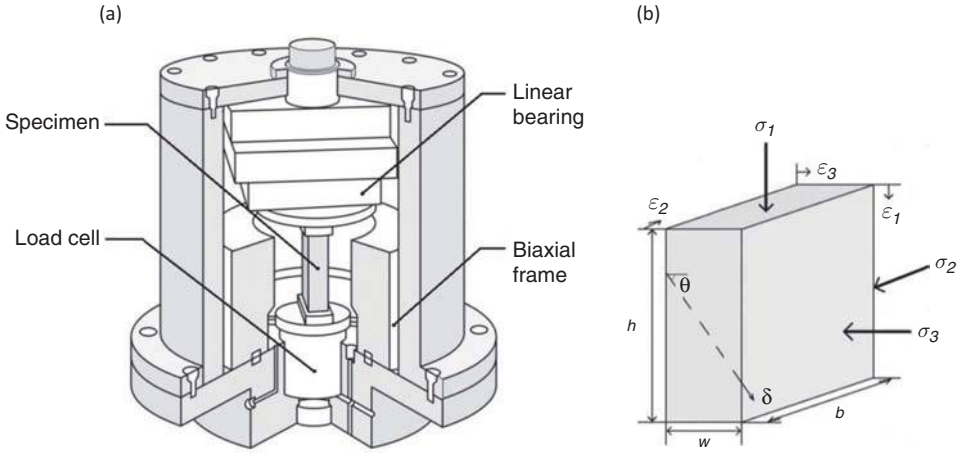

Figure 1 (a) University of Minnesota Plane Strain Apparatus; (b) Specimen geometry with principal stresses and corresponding strains.

with no restriction. The apparatus is internally instrumented with five pressure resistant LVDTs for measuring axial and lateral displacements, two load cells for measuring axial force, and four strain gages for measuring strains on the specimen and the deformation of the biaxial frame. The two surfaces of the specimen exposed to confining pressure are sealed by a polyurethane coating; metal targets glued to the specimen provide firm contact points for the lateral LVDTs. The four surfaces in contact with polished-steel platens are covered with a stearic acid lubricant to reduce frictional constraint (Labuz & Bridell, 1993).

2.1 Experiments

Plane strain experiments were performed on Red Wildmoor sandstone with a porosity of 25.8% and uniaxial compressive strength C_o = 10.0 MPa; the uniaxial test gave Young's modulus E = 2.0 GPa and Poisson's ratio ν = 0.34. The grains of the sandstone are subrounded with a mean grain diameter of 0.1 mm. Closed-loop, servo-controlled tests with lateral displacement as the feedback signal were conducted at confining pressures (σ_3) of 3.5 and 10.0 MPa. For convenience, force and displacement are taken positive for compression and shortening (*cf.* Jaeger *et al.*, 2007).

Figure 2 shows the axial load and lateral displacement responses as a function of axial displacement. The brittle nature of the rock is apparent for 3.5 MPa test; in post-peak, the axial force dropped sharply with little change in axial displacement (Figure 2a). In fact, the response of the axial displacement was to decrease or snap-back, which was possible to observe because of lateral displacement control. Note that this class II snapback behavior is not constitutive response but is due to the "system" containing the displacements along the failure plane and from the elastic unloading of the specimen, and these involve modulus, fracture parameters, and size (explained in Section 4). As confinement increased to 10 MPa, the global response was no longer class II; load reduced with a small increase in axial displacement to a residual level (Figure 2b). The orientations of the failure plane relative to the lateral (minimum stress) direction were 63° and 58°, an indication that dilatancy and friction are pressure dependent.

2.2 Dilatancy and friction

The major principal strains are calculated from the global displacements ($\varepsilon_1 = \varepsilon_{yy} = \Delta h/h$, $\varepsilon_2 = \varepsilon_{zz} = 0$, $\varepsilon_3 = \varepsilon_{xx} = \Delta w/w$) such that volume strain ε and shear strain γ are simply

$$\varepsilon = \varepsilon_1 + \varepsilon_3,\ \gamma = \varepsilon_1 - \varepsilon_3 \tag{1}$$

which can be decomposed into incremental elastic and plastic (inelastic) components:

$$\Delta\varepsilon = \Delta\varepsilon^e + \Delta\varepsilon^p,\ \Delta\gamma = \Delta\gamma^e + \Delta\gamma^p \tag{2}$$

The plastic strains were determined from the measured total strains and the calculated elastic strains (constant E, ν) at the start of nonlinear volume strain behavior (Riedel & Labuz, 2007), and the plastic volume response is shown in Figure 3a. The dilatancy angle ψ (Hansen, 1958) is determined by

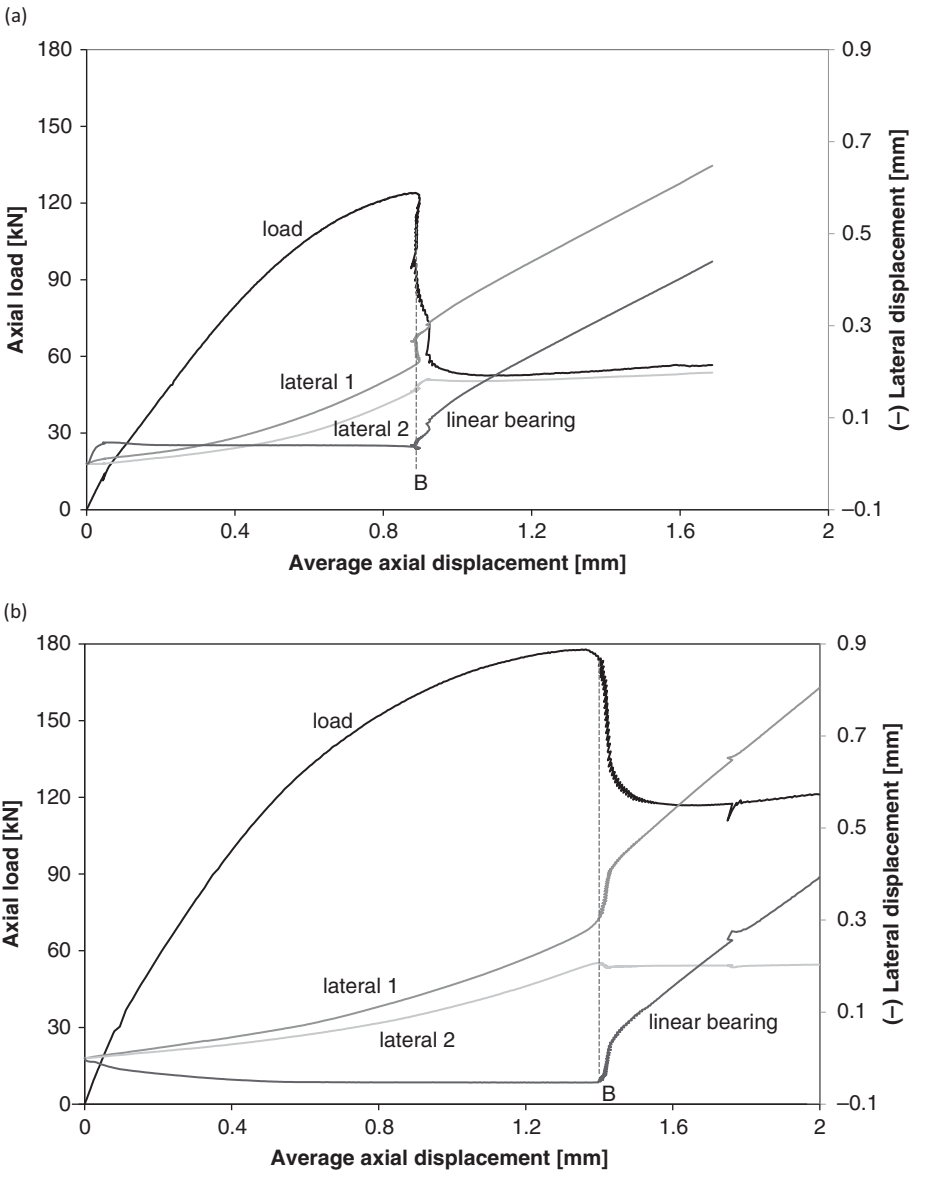

Figure 2 Load – displacement response of sandstone at (a) 3.5 MPa confinement and (b) 10.0 MPa confinement; the shear band traversed the specimen and slip displacement started at B.

$$\sin \psi = -\frac{\Delta \varepsilon^p}{\Delta \gamma^p} \tag{3}$$

and ψ as a function of plastic shear strain is illustrated in Figure 3b. At low confinement ($\sigma_3 = 0.35C_o$), the rock compacted very little before dilating and reached a dilation

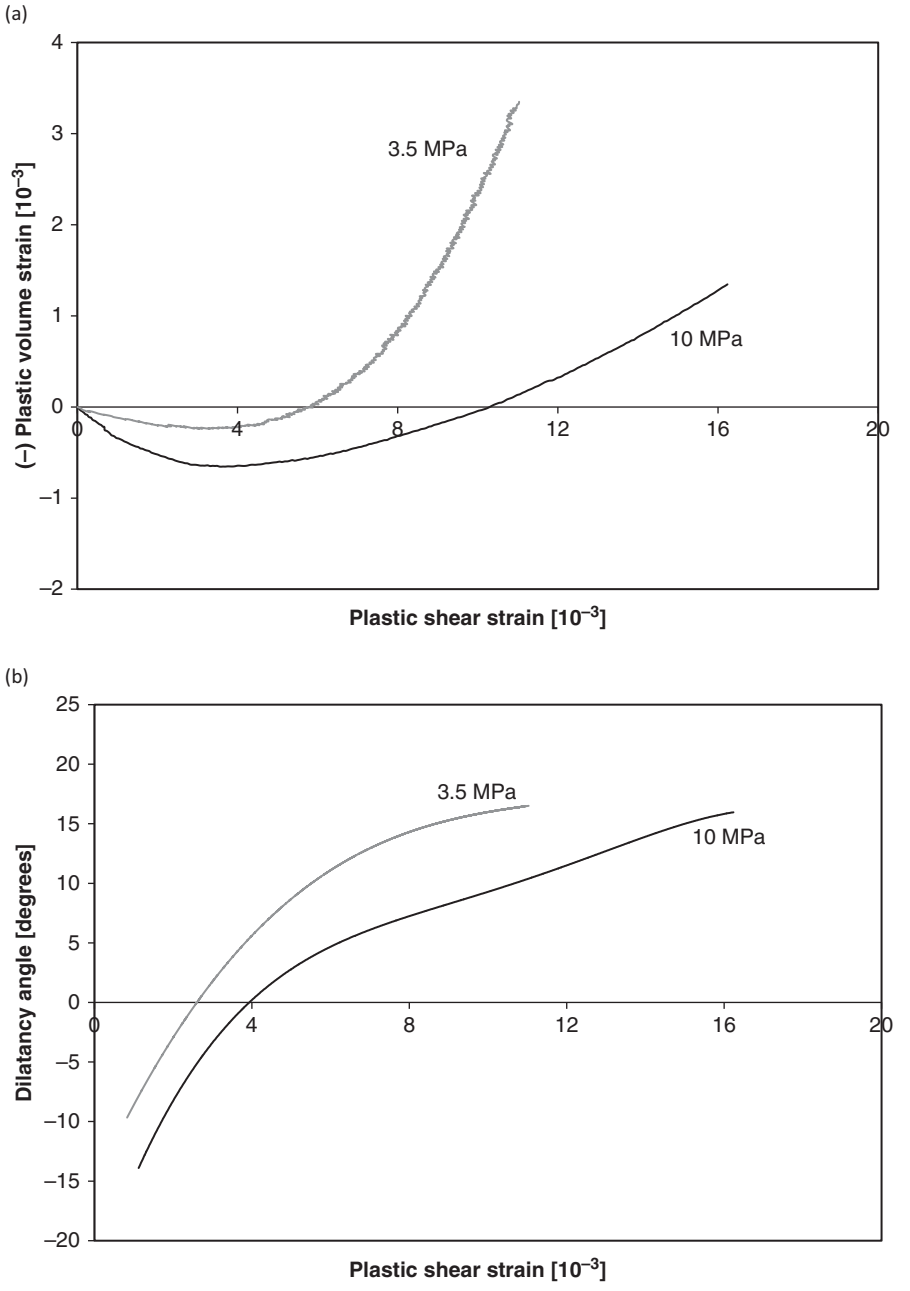

Figure 3 Behavior of the sandstone: (a) plastic volume response, (b) dilatancy angle.

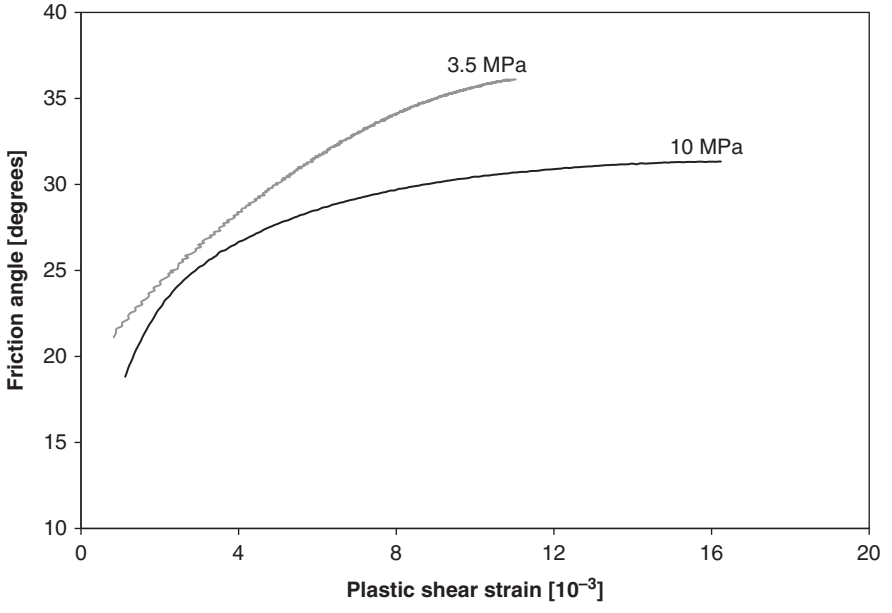

Figure 4 Mobilized friction angle at 3.5 MPa and 10.0 MPa confinement.

angle at peak stress $\psi = 17^{o}$. At high confinement ($\sigma_3 = C_o$), the sandstone displayed compaction followed by peak dilation $\psi = 14^{o}$.

The Mohr-Coulomb (MC) failure criterion can be written as

$$\sin \phi_m = \frac{t}{s - V_o} \tag{4}$$

where (2D) mean stress $s = (\sigma_1 + \sigma_3)/2$, shear stress $t = (\sigma_1 - \sigma_3)/2$, the parameter $V_o = S_o/\tan\phi_p$ is the intercept at $t = 0$, S_o is the shear stress intercept also known as cohesion c, and ϕ_p is the peak friction angle. The sandstone is assumed to have a linear yield envelope with constant V_o and increasing friction (and cohesion). The relationship between mobilized friction angle ϕ_m and plastic shear strain showed sensitivity to pressure (Figure 4): as pressure increased, ϕ_m decreased. Friction angles were different at the two confining pressures, suggesting a nonlinear failure envelope.

3 FAILURE CRITERIA

The MC criterion of Equation 4, which is a reasonable approximation in the brittle regime over a limited range of mean stress, can be written (a, c are material parameters):

$$a\sigma_1 + c\sigma_3 = 1 \tag{5}$$

which represents a plane in principal stress space σ_1, σ_2, σ_3, but it is natural to consider

$$A\sigma_1 + B\sigma_2 + C\sigma_3 = 1 \tag{6}$$

which is called Paul-Mohr-Coulomb (PMC) by Meyer & Labuz (2013). Note that PMC includes σ_2. PMC can be evaluated by performing conventional triaxial testing on a right circular cylinder, where axial (vertical) stress $\sigma_a = \sigma_V$ is applied independent of radial (horizontal) stress $\sigma_r = \sigma_H = \sigma_h$ so that either compression ($\sigma_r = \sigma_2 = \sigma_3$) or extension failure ($\sigma_r = \sigma_1 = \sigma_2$) can be achieved. The generalized pyramidal failure surface, Equation 6, was proposed by Paul (1968), a simple version by Haythornthwaite (1962), and it can be written as

$$\frac{\sigma_1}{V_o}\left[\frac{1-\sin\phi_c}{2\sin\phi_c}\right] + \frac{\sigma_2}{V_o}\left[\frac{\sin\phi_c - \sin\phi_e}{2\sin\phi_c \sin\phi_e}\right] - \frac{\sigma_3}{V_o}\left[\frac{1+\sin\phi_e}{2\sin\phi_e}\right] = 1 \tag{7}$$

where ϕ_c is the internal friction angle for compression ($\sigma_2 = \sigma_3$), ϕ_e is the internal friction angle for extension ($\sigma_2 = \sigma_1$), and V_o is the intersection of the failure surface with the hydrostatic axis ($\sigma_1 = \sigma_2 = \sigma_3$); V_o represents all-around equal tension and it is not measured in experiments.

For isotropic rock, the orientation of the principal stresses does not matter and they can be relabeled as σ_V, σ_H, σ_h and interchanged as major, intermediate, and minor principal stresses. Because of the six orderings of the principal stresses, six planes can be constructed in σ_V, σ_H, σ_h space giving an irregular hexagonal pyramid (Figure 5a). The plane normal to the hydrostatic axis is called the π-plane and the projections of the coordinate axes are labeled σ'_V, σ'_H, σ'_h (Figure 5b); stress paths are shown for conventional triaxial compression and extension, and plane strain compression.

As reported in Table 1, triaxial compression and extension data from Papamichos *et al.* (2000), along with the plane strain data, were used to find the best-fit plane (Figure 6a) and the coefficients *A, B, C* (Makhnenko *et al.*, 2015); note that because of isotropy, the extension data can be "moved" to the plane containing the compression

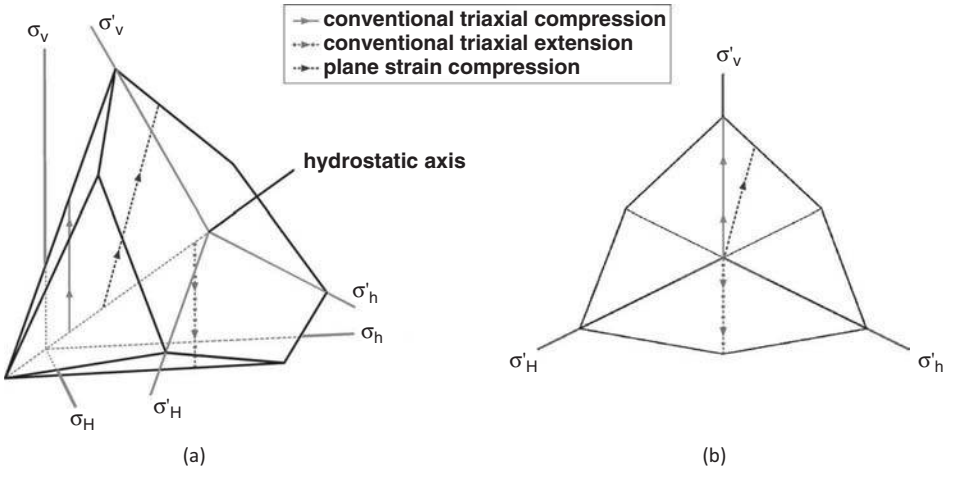

Figure 5 Linear failure surfaces with stress paths in (a) principal stress space, (b) π-plane view.

Table 1 Principal stresses at failure for plane strain compression (BXC) and conventional triaxial compression (TXCO) and extension (TXEX) experiments.

Test name	σ_1 *[MPa]*	σ_2 *[MPa]*	σ_3 *[MPa]*
BXC-1	17.0	7.8	0.4
BXC-2	33.4	12.3	3.5
BXC-3	56.0	22.5	10.0
TXCO-1	15.1	0.4	0.4
TXCO-2	21.3	1.4	1.4
TXCO-3	30.0	3.5	3.5
TXCO-4	41.7	6.9	6.9
TXCO-5	49.8	10.3	10.3
TXEX-6	60.0	60.0	8.1
TXEX -7	52.5	52.5	5.9
TXEX -8	48.0	48.0	4.4
TXEX -9	45.0	45.0	3.3

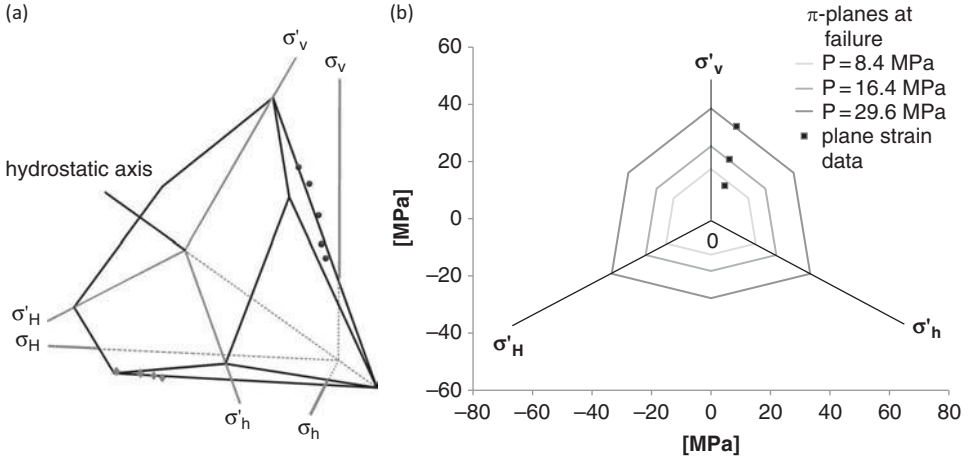

Figure 6 PMC failure surface and data for sandstone. (a) principal stress space with diamonds and circles from triaxial extension and compression. (b) π-plane view with plane strain data.

data. The friction angles in compression and extension are $\phi_c = 30.6°$ and $\phi_e = 37.8°$, demonstrating an intermediate stress effect for the rock. From the vertex $V_o = 8.7$ MPa, the cohesions in compression and extension are $c_c = 5.3$ MPa and $c_e = 7.0$ MPa. The view in the π-plane showing the plane strain data is given in Figure 6b.

4 SOFTENING

Figure 7 shows a close-up of the mechanical response around peak load, including the decrease in force with increase in lateral displacement known as softening, although this is not material response because of the failure process. From observations of

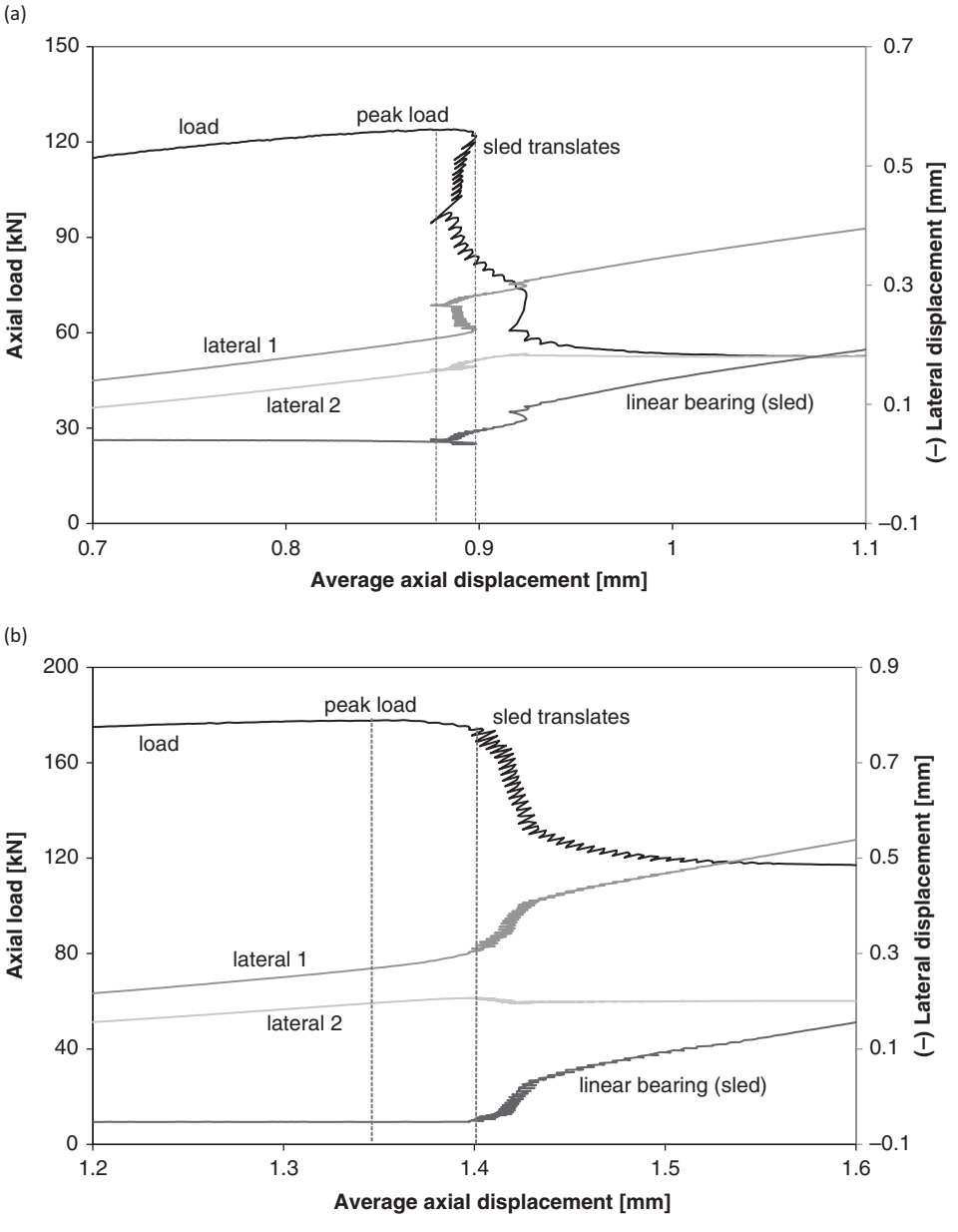

Figure 7 Load – displacement response of the sandstone around peak load at (a) 3.5 MPa confinement showing class II behavior and (b) 10.0 MPa confinement showing class I.

acoustic emission locations and optical microscopy, it is clear that strain localization – the shear band – is formed at or slightly before peak load but it does not traverse the specimen (Carvalho & Labuz, 2002; Labuz *et al.*, 2006); propagation of the shear band (unstable crack growth) is responsible for initial softening after peak. Once a mechanism

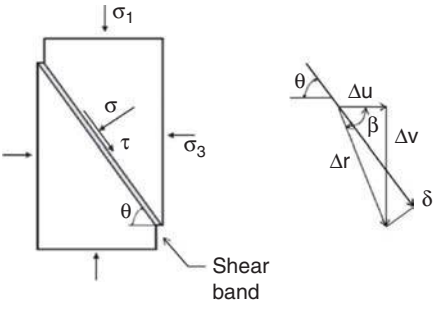

Figure 8 Loading and kinematics of the shear band.

is formed, which means that the shear band is fully developed, the upper block slides with a normal component associated with either compaction or dilation (Figure 8).

4.1 Shear band characteristics

From the plane strain experiments, the softening response of the specimen (Figure 8) with the shear band angle θ, measured from σ_3, can be determined from the shear stress $\tau = t(sin2\theta)$ and slip displacement δ:

$$\delta = [(\Delta u)^2 + (\Delta v)^2]^{1/2} \tag{8}$$

where Δu is the lateral displacement of the upper block sliding along the shear band and Δv is the axial component of sliding (Figure 9a). The angle β is the orientation of the resultant displacement $\Delta r = [(\Delta u)^2 + (\Delta v)^2]^{1/2}$:

$$\cos \beta = \frac{\Delta u}{\Delta r} \tag{9}$$

For both experiments, the shear band compacted (negative dilation) with slip before reaching the residual value of zero dilation (Figure 9b). For the 10 MPa experiment, Figure 10 describes how the shear stress degraded from a value τ_p corresponding to the onset of slip (not at peak force) to a constant residual level τ_r, when δ exceeds a critical amount of slip $\delta_c = 0.35$ mm for this sandstone. The energy per unit area dissipated along the shear band is (Palmer & Rice, 1973; Rice, 1980; Wong, 1982)

$$G_c = \int_0^{\delta_c} (\tau - \tau_r) d\delta \tag{10}$$

given by $G_c = 1.14$ kJ/m^2. A summary of the material and shear band characteristics is contained in Table 2, along with data from an additional experiment performed at $\sigma_3 = 15.0$ MPa.

4.2 Stability analysis

To explain the softening response for the plane strain compression test, we modify the plane stress analysis presented by Labuz & Biolzi (1991). Once the shear band develops

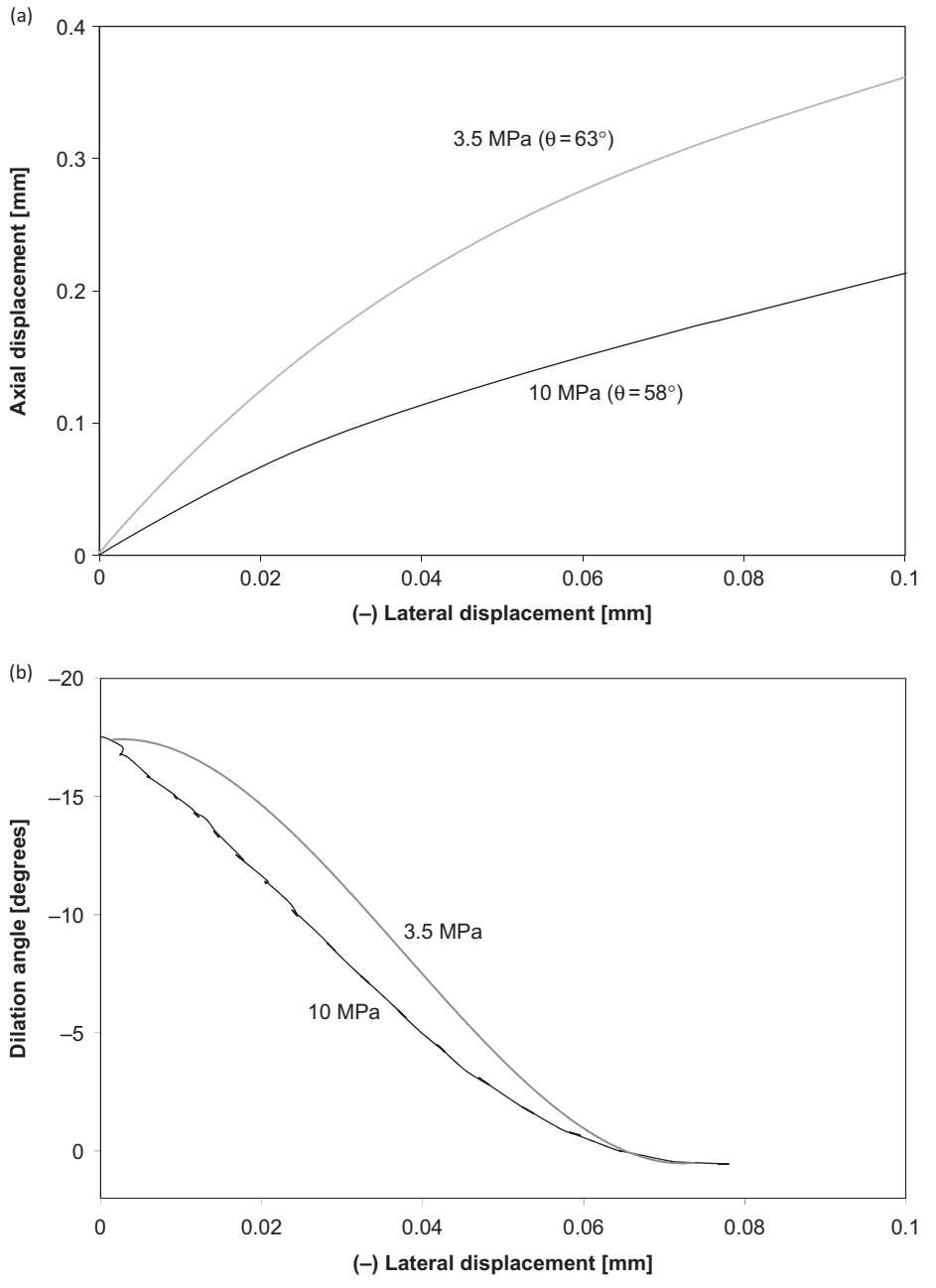

Figure 9 Shear band (a) kinematics and (b) dilation angle for the sandstone.

across the entire specimen, further displacement involves the rock outside the band unloading elastically, while rock inside the band deforms such as to give a net slip δ with decreasing stress τ. The relation between δ and τ follows the slip-weakening model of Palmer & Rice (1973), where the shear stress decreases from a value τ_p at the start of

Table 2 Summary of the sandstone parameters from plane strain experiments.

Parameter	*3.5 MPa*	*10 MPa*	*15 MPa*
Dilatancy angle (peak)	17	14	10
Friction angle (peak)	36	31	29
Shear band angle	63	58	52
Residual /peak shear stress	0.43	0.66	0.88
Critical slip displacement [mm]	0.40	0.35	0.27
Dissipated energy [kJ/m^2]	0.83	1.14	0.22
Brittleness number	0.96	1.46	1.56

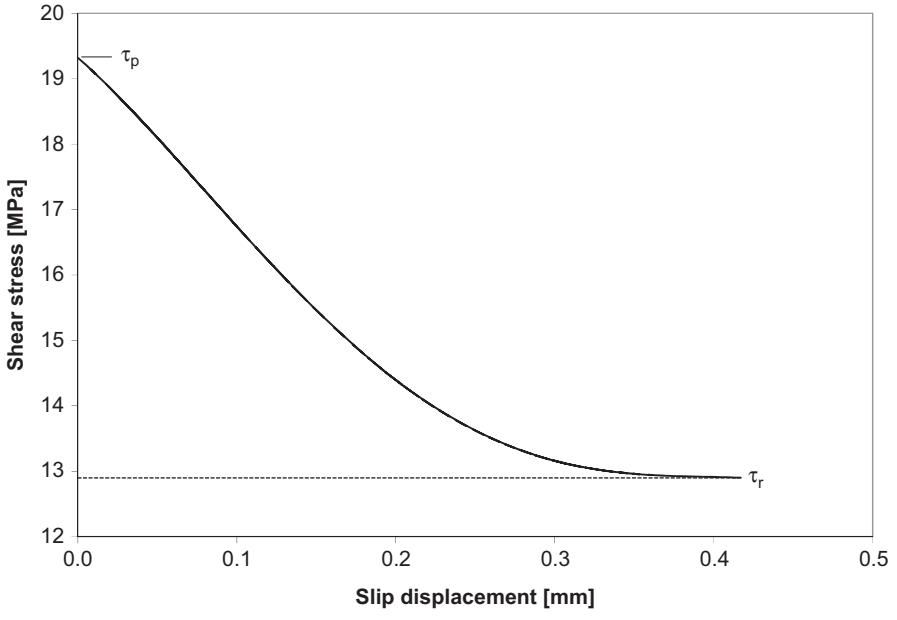

Figure 10 Slip weakening law of the sandstone at 10 MPa confinement.

slip to the residual value τ_r at a critical amount of slip δ_c. The behavior shown in Figure 10 is approximated by a linear function:

$$\delta = \delta_c \left(1 - \frac{\Delta\tau}{\Delta\tau_p}\right) \tag{11}$$

where $\Delta\tau = \tau - \tau_r$ and $\Delta\tau_p = \tau_p - \tau_r$.

Consider the plane strain specimen of height h and width w that behaves linearly up to peak load, at which point a shear band of angle θ forms with the slip-weakening constitutive relation. The total displacement v is due to the rock, testing machine, and shear band:

$$v = \frac{h}{2\mu}[\Delta\sigma(1-\nu) + \sigma_3(1-2\nu)] + \frac{w}{k'}(\Delta\sigma + \sigma_3) + \delta_c\left(1 - \frac{\Delta\tau}{\Delta\tau_p}\right)\sin\theta \tag{12}$$

where $\Delta\sigma = \sigma_1 - \sigma_3$, μ = shear modulus, $2\mu = E/(1 + \nu)$, and k' is the testing machine (load frame) stiffness per unit thickness b.

Apply the incremental stability condition for critical softening $dv/d\Delta\sigma = 0$ to Equation 12:

$$h\frac{(1-\nu)}{2\mu} + \frac{w}{k'} = \frac{\delta_c \sin^2\theta \cos\theta}{\tau_p - \tau_r} \tag{13}$$

where $\tau = \Delta\sigma \sin\theta \cos\theta$. Because fracture energy and Young's modulus are more readily identified than critical slip displacement and shear modulus, it is convenient to substitute G_f for δ_c and E for μ, with $f(\theta) = \sin 2\theta \sin\theta$, $\lambda = h/w$, $E' = E/(1 - \nu^2)$ and the final result is

$$\frac{1}{f(\theta)}\left(\lambda + \frac{E'}{k'}\right) = \frac{G_f E'}{w(\tau_p - \tau_r)^2} \tag{14}$$

A number of interesting features in Equation 14 are noted:

- Material properties, specimen size and shape, as well as confinement (mean stress), which influences both G_f and $(\tau_p - \tau_r)$, are important for determining stability.
- Machine stiffness influences the post-peak response, but it is not the sole factor. Even for an infinitely stiff machine, a class II behavior can still be observed.
- A brittleness number $B_n = G_f E'/[w(\tau_p - \tau_r)^2]$ appears with a size dependence, such that for specimens smaller or larger than some width w and the same material properties E', G_f, and $(\tau_p - \tau_r)$, the response is stable for small w and unstable for large.
- The LHS > RHS in Equation 14 predicts class II response, and the smallest B_n is associated with the 3.5 MPa experiment (Table 2), which exhibited class II behavior.

5 SUMMARY

The material and softening behavior of rock can be studied using a Vardoulakis-Goldscheider plane strain apparatus, which combines the positive features of a constitutive (plane strain) compression test, such that the two-dimensional material behavior, including dilatancy and friction, can be evaluated, and a direct shear test, such that the shear stress-slip displacement and dilatancy characteristics of the shear band can be measured. Although the nature of the inelasticity (microcracking, intergranular sliding, etc.) was not identified, the inelastic (plastic) response can be determined by removing the elastic response, in an incremental approach.

The softening behavior of a rock is not an essential material property but simply a typical global response, as failure occurs in a manner described by the slip-weakening model of fracture. Furthermore, the stability is dependent not only on machine stiffness, but also on geometry and size of the specimen.

REFERENCES

Carvalho, F. & Labuz, J.F. 2002. Moment tensors of acoustic emission in shear faulting under plane-strain compression. *Tectonophysics*, 356, 199–211.

Drescher, A., Vardoulakis, I. & Han, C. 1990. A biaxial apparatus for testing soils. *Geotech. Testing J. ASTM* 13, 226–234.

Hansen, B. 1958. Line ruptures regarded as narrow rupture zones. Basic equations based on kinematic considerations. *Proc. Conf. Earth Pressure Problems*. Brussels, 1, pp. 39–48.

Haythornthwaite, R.M. 1962. Range of yield condition in ideal plasticity. *Trans. ASCE*, 127(I), 1252–1267.

Jaeger, J.C., Cook, N.G.W. & Zimmerman, R.W. 2007. *Fundamentals of Rock Mechanics, 4th edn*. London, Blackwell.

Labuz, J.F. & Biolzi, L. 1991. Class I vs. class II stability: a demonstration of size effect. *Int. J. Rock Mech. Min. Sci. Geomech. Abstr.*, 28, 199–205.

Labuz, J.F. & Bridell, J.M. 1993. Reducing frictional constraint in compression testing through lubrication. *Int. J. Rock Mech. Min. Sci. Geomech. Abstr.*, 30, 451–455.

Labuz, J.F., Dai, S.-T. & Papamichos, E. 1996. Plane-strain compression of rock-like materials. *Int. J. Rock Mech. Min. Sci. Geomech. Abstr.* 33, 573–584.

Labuz, J.F., Riedel, J.J. & Dai, S.-T. 2006. Shear fracture in sandstone under plane strain compression. *Eng. Frac. Mech.* 73, 820–828.

Makhnenko, R. & Labuz, J. 2014. Plane strain testing with passive restraint. *Rock Mech. Rock Eng.*, 47(6), 2021–2029.

Makhnenko, R.Y., Harvieux, J. & Labuz, J.F. 2015. Paul-Mohr-Coulomb failure surface of rock in the brittle regime. *Geophys. Res. Lett.*, 42, 6975–6981.

Meyer, J.P. & Labuz, J.F. 2013. Linear failure criteria with three principal stresses. *Int. J. Rock Mech. Min. Sci.*, 60, 180–187.

Nadai, A. 1950. *Theory of Flow and Fracture of Solids*. New York, McGraw-Hill.

Palmer, A.C. & Rice, J.R. 1973. The growth of slip surfaces in the progressive failure of over-consolidated clay. *Proc. Roy. Soc. Lond. A*, 332, 527–548.

Papamichos, E., Tronvoll, J. Skjvstein, A., Unander, T.E., Labuz, J.F., Vardoulakis, I. & Sulem, J. 2000. Constitutive testing of Red Wildmoor sandstone. *Mech. Cohes. Frict. Mater.*, 5, 1–40.

Paul, B. 1968. Generalized pyramidal fracture and yield criteria. *Int. J. Solids Struct.*, 4, 175–196.

Rice, J.R. 1980. The mechanics of earthquake rupture. In: Dziewonski, A.M. & Boschi, E. (eds.) *Physics of the Earth's Interior, Italian Physical Society, Bologna*. Amsterdam, North-Holland. pp. 555–649.

Riedel, J.J. & Labuz, J.F., 2007. Propagation of a shear band in sandstone. *Int J. Num. Anal. Meth. Geomech.*, 31, 1281–1299.

Vardoulakis, I. & Goldscheider, M. 1981. Biaxial apparatus for testing shear bands in soils. *Proc. 10th Int. Conf. Soil Mech. Found. Eng.* Rotterdam, Balkema. pp. 819–824

Vardoulakis, I. & Sulem, J. 1995. *Bifurcation Analysis in Geomechanics*. Glasgow, Blackie Academic & Professional.

Wong, T.F. 1982. Shear fracture energy of Westerly granite from post-failure behavior. *J. Geophys. Res.* 87, 990–1000.